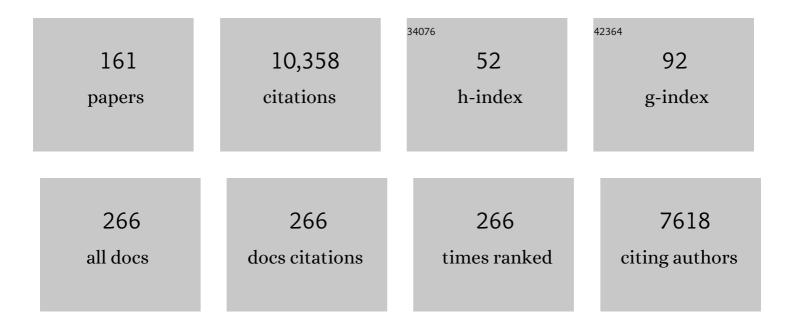
## Lieven Clarisse

List of Publications by Year in descending order

Source: https://exaly.com/author-pdf/6609091/publications.pdf Version: 2024-02-01



#	Article	IF	CITATIONS
1	Monitoring of atmospheric composition using the thermal infrared IASI/MetOp sounder. Atmospheric Chemistry and Physics, 2009, 9, 6041-6054.	1.9	694
2	Global ammonia distribution derived from infrared satellite observations. Nature Geoscience, 2009, 2, 479-483.	5.4	400
3	Hyperspectral Earth Observation from IASI: Five Years of Accomplishments. Bulletin of the American Meteorological Society, 2012, 93, 347-370.	1.7	357
4	The 2010 explosive eruption of Java's Merapi volcano—A â€~100-year' event. Journal of Volcanology and Geothermal Research, 2012, 241-242, 121-135.	0.8	336
5	Determination of time- and height-resolved volcanic ash emissions and their use for quantitative ash dispersion modeling: the 2010 Eyjafjallajökull eruption. Atmospheric Chemistry and Physics, 2011, 11, 4333-4351.	1.9	333
6	Towards a climate-dependent paradigm of ammonia emission and deposition. Philosophical Transactions of the Royal Society B: Biological Sciences, 2013, 368, 20130166.	1.8	328
7	Industrial and agricultural ammonia point sources exposed. Nature, 2018, 564, 99-103.	13.7	312
8	Stratospheric aerosol-Observations, processes, and impact on climate. Reviews of Geophysics, 2016, 54, 278-335.	9.0	265
9	Atmospheric ammonia and particulate inorganic nitrogen over the United States. Atmospheric Chemistry and Physics, 2012, 12, 10295-10312.	1.9	240
10	Multi-decadal satellite measurements of global volcanic degassing. Journal of Volcanology and Geothermal Research, 2016, 311, 99-134.	0.8	234
11	Global distributions, time series and error characterization of atmospheric ammonia (NH <sub>3</sub> ) from IASI satellite observations. Atmospheric Chemistry and Physics, 2014, 14, 2905-2922.	1.9	195
12	Strong constraints on aerosol–cloud interactions from volcanic eruptions. Nature, 2017, 546, 485-491.	13.7	191
13	Satellite evidence for a large source of formic acid from boreal and tropical forests. Nature Geoscience, 2012, 5, 26-30.	5.4	171
14	IASI measurements of reactive trace species in biomass burning plumes. Atmospheric Chemistry and Physics, 2009, 9, 5655-5667.	1.9	165
15	FORLI radiative transfer and retrieval code for IASI. Journal of Quantitative Spectroscopy and Radiative Transfer, 2012, 113, 1391-1408.	1.1	162
16	Ammonia Emissions May Be Substantially Underestimated in China. Environmental Science & Technology, 2017, 51, 12089-12096.	4.6	160
17	Volcanic SO <sub>2</sub> fluxes derived from satellite data: a survey using OMI, GOME-2, IASI and MODIS. Atmospheric Chemistry and Physics, 2013, 13, 5945-5968.	1.9	151
18	Retrieval of sulphur dioxide from the infrared atmospheric sounding interferometer (IASI). Atmospheric Measurement Techniques, 2012, 5, 581-594.	1.2	150

#	Article	IF	CITATIONS
19	Characterization of methane retrievals from the IASI space-borne sounder. Atmospheric Chemistry and Physics, 2009, 9, 7889-7899.	1.9	148
20	Tracking and quantifying volcanic SO <sub>2</sub> with IASI, the September 2007 eruption at Jebel at Tair. Atmospheric Chemistry and Physics, 2008, 8, 7723-7734.	1.9	136
21	Development, Production and Evaluation of Aerosol Climate Data Records from European Satellite Observations (Aerosol_cci). Remote Sensing, 2016, 8, 421.	1.8	131
22	TES ammonia retrieval strategy and global observations of the spatial and seasonal variability of ammonia. Atmospheric Chemistry and Physics, 2011, 11, 10743-10763.	1.9	129
23	Observations of the eruption of the Sarychev volcano and simulations using the HadGEM2 climate model. Journal of Geophysical Research, 2010, 115, .	3.3	128
24	First space-based derivation of the global atmospheric methanol emission fluxes. Atmospheric Chemistry and Physics, 2011, 11, 4873-4898.	1.9	122
25	Satellite monitoring of ammonia: A case study of the San Joaquin Valley. Journal of Geophysical Research, 2010, 115, .	3.3	118
26	Version 2 of the IASI NH <sub>3</sub> neural network retrieval algorithm: near-real-time and reanalysed datasets. Atmospheric Measurement Techniques, 2017, 10, 4905-4914.	1.2	118
27	Detection of volcanic SO <sub>2</sub> , ash, and H <sub>2</sub> SO <sub>4</sub> using the Infrared Atmospheric Sounding Interferometer (IASI). Journal of Geophysical Research, 2010, 115, .	3.3	117
28	A unified approach to infrared aerosol remote sensing and type specification. Atmospheric Chemistry and Physics, 2013, 13, 2195-2221.	1.9	105
29	A flexible and robust neural network IASIâ€NH <sub>3</sub> retrieval algorithm. Journal of Geophysical Research D: Atmospheres, 2016, 121, 6581-6599.	1.2	96
30	Evaluating the structure and magnitude of the ash plume during the initial phase of the 2010 EyjafjallajA¶kull eruption using lidar observations and NAME simulations. Journal of Geophysical Research, 2011, 116, .	3.3	93
31	The 2011 Nabro eruption, a SO <sub>2</sub> plume height analysis using IASI measurements. Atmospheric Chemistry and Physics, 2014, 14, 3095-3111.	1.9	93
32	Towards validation of ammonia (NH <sub>3</sub> ) measurements from the IASI satellite. Atmospheric Measurement Techniques, 2015, 8, 1575-1591.	1.2	90
33	NH <sub>3</sub> emissions from large point sources derived from CrIS and IASI satellite observations. Atmospheric Chemistry and Physics, 2019, 19, 12261-12293.	1.9	89
34	Thermal infrared nadir observations of 24 atmospheric gases. Geophysical Research Letters, 2011, 38, n/a-n/a.	1.5	88
35	Support to Aviation Control Service (SACS): an online service for near-real-time satellite monitoring of volcanic plumes. Natural Hazards and Earth System Sciences, 2014, 14, 1099-1123.	1.5	85
36	The infrared spectral signature of volcanic ash determined from high-spectral resolution satellite measurements. Remote Sensing of Environment, 2010, 114, 414-425.	4.6	82

#	Article	IF	CITATIONS
37	A correlation method for volcanic ash detection using hyperspectral infrared measurements. Geophysical Research Letters, 2010, 37, .	1.5	82
38	Retrieving radius, concentration, optical depth, and mass of different types of aerosols from high-resolution infrared nadir spectra. Applied Optics, 2010, 49, 3713.	2.1	80
39	Sulfur dioxide vertical column DOAS retrievals from the Ozone Monitoring Instrument: Global observations and comparison to groundâ€based and satellite data. Journal of Geophysical Research D: Atmospheres, 2015, 120, 2470-2491.	1.2	79
40	Ammonia emissions in tropical biomass burning regions: Comparison between satellite-derived emissions and bottom-up fire inventories. Atmospheric Environment, 2015, 121, 42-54.	1.9	78
41	Exceptional emissions of NH <sub>3</sub> and HCOOH in the 2010 Russian wildfires. Atmospheric Chemistry and Physics, 2013, 13, 4171-4181.	1.9	76
42	H <sub>2</sub> <sup>16</sup> O and HDO measurements with IASI/MetOp. Atmospheric Chemistry and Physics, 2009, 9, 9433-9447.	1.9	74
43	Global distributions of methanol and formic acid retrieved for the first time from the IASI/MetOp thermal infrared sounder. Atmospheric Chemistry and Physics, 2011, 11, 857-872.	1.9	71
44	Ubiquitous atmospheric production of organic acids mediated by cloud droplets. Nature, 2021, 593, 233-237.	13.7	71
45	Separation of ash and sulfur dioxide during the 2011 GrĀmsv¶tn eruption. Journal of Geophysical Research D: Atmospheres, 2014, 119, 7477-7501.	1.2	69
46	Satellite Monitoring of Volcanic Sulfur Dioxide Emissions for Early Warning of Volcanic Hazards. IEEE Journal of Selected Topics in Applied Earth Observations and Remote Sensing, 2009, 2, 196-206.	2.3	67
47	Worldwide spatiotemporal atmospheric ammonia (NH <sub>3</sub> ) columns variability revealed by satellite. Geophysical Research Letters, 2015, 42, 8660-8668.	1.5	66
48	Global, regional and national trends of atmospheric ammonia derived from a decadal (2008–2018) satellite record. Environmental Research Letters, 2021, 16, 055017.	2.2	65
49	A physics-based approach to oversample multi-satellite, multispecies observations to a common grid. Atmospheric Measurement Techniques, 2018, 11, 6679-6701.	1.2	64
50	The unintended consequence of SO <sub>2</sub> and NO <sub>2</sub> regulations over China: increase of ammonia levels and impact on PM <sub>2.5</sub> concentrations. Atmospheric Chemistry and Physics, 2019, 19, 6701-6716.	1.9	63
51	Mid-tropospheric Î'D observations from IASI/MetOp at high spatial and temporal resolution. Atmospheric Chemistry and Physics, 2012, 12, 10817-10832.	1.9	62
52	Evaluating 4 years of atmospheric ammonia (NH <sub>3</sub> ) over Europe using IASI satellite observations and LOTOSâ€EUROS model results. Journal of Geophysical Research D: Atmospheres, 2014, 119, 9549-9566.	1.2	61
53	Record high levels of atmospheric ammonia over India: Spatial and temporal analyses. Science of the Total Environment, 2020, 740, 139986.	3.9	61
54	Ash and sulfur dioxide in the 2008 eruptions of Okmok and Kasatochi: Insights from high spectral resolution satellite measurements. Journal of Geophysical Research, 2010, 115, .	3.3	59

#	Article	IF	CITATIONS
55	Sulfur dioxide layer height retrieval from Sentinel-5 Precursor/TROPOMI using FP_ILM. Atmospheric Measurement Techniques, 2019, 12, 5503-5517.	1.2	58
56	First simultaneous space measurements of atmospheric pollutants in the boundary layer from IASI: A case study in the North China Plain. Geophysical Research Letters, 2014, 41, 645-651.	1.5	57
57	An evaluation of IASI-NH <sub>3</sub> with ground-based Fourier transform infrared spectroscopy measurements. Atmospheric Chemistry and Physics, 2016, 16, 10351-10368.	1.9	56
58	Temporal and spatial variability of ammonia in urban and agricultural regions of northern Colorado, United States. Atmospheric Chemistry and Physics, 2017, 17, 6197-6213.	1.9	53
59	Global nitrous acid emissions and levels of regional oxidants enhanced by wildfires. Nature Geoscience, 2020, 13, 681-686.	5.4	51
60	Interannual variability of ammonia concentrations over the United States: sources and implications. Atmospheric Chemistry and Physics, 2016, 16, 12305-12328.	1.9	48
61	Measuring volcanic degassing of SO2 in the lower troposphere with ASTER band ratios. Journal of Volcanology and Geothermal Research, 2010, 194, 42-54.	0.8	47
62	A case study of observations of volcanic ash from the Eyjafjallajökull eruption: 2. Airborne and satellite radiative measurements. Journal of Geophysical Research, 2012, 117, .	3.3	47
63	Inverting for volcanic SO <sub>2</sub> flux at high temporal resolution using spaceborne plume imagery and chemistry-transport modelling: the 2010 Eyjafjallajökull eruption case study. Atmospheric Chemistry and Physics, 2013, 13, 8569-8584.	1.9	46
64	IASI observations of sulfur dioxide (SO <sub>2</sub> ) in the boundary layer of Norilsk. Journal of Geophysical Research D: Atmospheres, 2014, 119, 4253-4263.	1.2	42
65	Doubling of annual ammonia emissions from the peat fires in Indonesia during the 2015 El Niño. Geophysical Research Letters, 2016, 43, 11,007.	1.5	41
66	Tropospheric methanol observations from space: retrieval evaluation and constraints on the seasonality of biogenic emissions. Atmospheric Chemistry and Physics, 2012, 12, 5897-5912.	1.9	39
67	Tracking down global NH <sub>3</sub> point sources with wind-adjusted superresolution. Atmospheric Measurement Techniques, 2019, 12, 5457-5473.	1.2	39
68	A General Framework for Global Retrievals of Trace Gases From IASI: Application to Methanol, Formic Acid, and PAN. Journal of Geophysical Research D: Atmospheres, 2018, 123, 13,963.	1.2	38
69	Measurements of SO <sub>2</sub> profiles in volcanic plumes from the NASA Tropospheric Emission Spectrometer (TES). Geophysical Research Letters, 2008, 35, .	1.5	37
70	Mixing of dust and NH <sub>3</sub> observed globally over anthropogenic dust sources. Atmospheric Chemistry and Physics, 2012, 12, 7351-7363.	1.9	37
71	Stratospheric aerosols from the Sarychev volcano eruption in the 2009 Arctic summer. Atmospheric Chemistry and Physics, 2013, 13, 6533-6552.	1.9	37
72	Unaccounted variability in NH 3 agricultural sources detected by IASI contributing to European spring haze episode. Geophysical Research Letters, 2016, 43, 5475-5482.	1.5	37

#	Article	IF	CITATIONS
73	Retrieval of near-surface sulfur dioxide (SO <sub>2</sub> ) concentrations at a global scale using IASI satellite observations. Atmospheric Measurement Techniques, 2016, 9, 721-740.	1.2	36
74	First satellite detection of volcanic OClO after the eruption of Puyehueâ€Cordón Caulle. Geophysical Research Letters, 2014, 41, 667-672.	1.5	35
75	Infrared satellite observations of hydrogen sulfide in the volcanic plume of the August 2008 Kasatochi eruption. Geophysical Research Letters, 2011, 38, n/a-n/a.	1.5	34
76	The sulfur budget of the 2011 GrÃmsvötn eruption, Iceland. Geophysical Research Letters, 2013, 40, 6095-6100.	1.5	33
77	Construction of bound entangled edge states with special ranks. Physics Letters, Section A: General, Atomic and Solid State Physics, 2006, 359, 603-607.	0.9	32
78	Intercontinental transport of anthropogenic sulfur dioxide and other pollutants: An infrared remote sensing case study. Geophysical Research Letters, 2011, 38, n/a-n/a.	1.5	32
79	Long-range transport of stratospheric aerosols in the Southern Hemisphere following the 2015 Calbuco eruption. Atmospheric Chemistry and Physics, 2017, 17, 15019-15036.	1.9	32
80	A Decadal Data Set of Global Atmospheric Dust Retrieved From IASI Satellite Measurements. Journal of Geophysical Research D: Atmospheres, 2019, 124, 1618-1647.	1.2	32
81	Ammonia and PM2.5 Air Pollution in Paris during the 2020 COVID Lockdown. Atmosphere, 2021, 12, 160.	1.0	32
82	Long-term trends in air quality in major cities in the UK and India: a view from space. Atmospheric Chemistry and Physics, 2021, 21, 6275-6296.	1.9	31
83	Rapid rise in premature mortality due to anthropogenic air pollution in fast-growing tropical cities from 2005 to 2018. Science Advances, 2022, 8, eabm4435.	4.7	31
84	Entangling power of permutations. Physical Review A, 2005, 72, .	1.0	30
85	Gasâ€aerosol partitioning of ammonia in biomass burning plumes: Implications for the interpretation of spaceborne observations of ammonia and the radiative forcing of ammonium nitrate. Geophysical Research Letters, 2017, 44, 8084-8093.	1.5	30
86	Validation of IASI Satellite Ammonia Observations at the Pixel Scale Using In Situ Vertical Profiles. Journal of Geophysical Research D: Atmospheres, 2021, 126, e2020JD033475.	1.2	28
87	A comparison of atmospheric dispersion model predictions with observations of SO <sub>2</sub> and sulphate aerosol from volcanic eruptions. Journal of Geophysical Research, 2012, 117, .	3.3	26
88	Aerosol properties of the Eyjafjallajökull ash derived from sun photometer and satellite observations over the Iberian Peninsula. Atmospheric Environment, 2012, 48, 22-32.	1.9	26
89	Unprecedented Atmospheric Ammonia Concentrations Detected in the High Arctic From the 2017 Canadian Wildfires. Journal of Geophysical Research D: Atmospheres, 2019, 124, 8178-8202.	1.2	25
90	Initial constraints on triggering mechanisms of the eruption of Fuego volcano (Guatemala) from 3 June 2018 using IASI satellite data. Journal of Volcanology and Geothermal Research, 2019, 376, 54-61.	0.8	25

#	Article	IF	CITATIONS
91	Atmospheric ammonia (NH3) emanations from Lake Natron's saline mudflats. Scientific Reports, 2019, 9, 4441.	1.6	24
92	Atmospheric ammonia variability and link with particulate matter formation: a case study over the Paris area. Atmospheric Chemistry and Physics, 2020, 20, 577-596.	1.9	24
93	UK Ammonia Emissions Estimated With Satellite Observations and GEOSâ€Chem. Journal of Geophysical Research D: Atmospheres, 2021, 126, e2021JD035237.	1.2	24
94	IASI's sensitivity to near-surface carbon monoxide (CO): Theoretical analyses and retrievals on test cases. Journal of Quantitative Spectroscopy and Radiative Transfer, 2017, 189, 428-440.	1.1	23
95	High-resolution hybrid inversion of IASI ammonia columns to constrain US ammonia emissions using the CMAQ adjoint model. Atmospheric Chemistry and Physics, 2021, 21, 2067-2082.	1.9	22
96	Tracking pollutants from space: Eight years of IASI satellite observation. Comptes Rendus - Geoscience, 2015, 347, 134-144.	0.4	21
97	Spaceborne Measurements of Formic and Acetic Acids: A Global View of the Regional Sources. Geophysical Research Letters, 2020, 47, e2019GL086239.	1.5	21
98	10-year satellite-constrained fluxes of ammonia improve performance of chemistry transport models. Atmospheric Chemistry and Physics, 2021, 21, 4431-4451.	1.9	21
99	Improving volcanic sulfur dioxide cloud dispersal forecasts by progressive assimilation of satellite observations. Geophysical Research Letters, 2014, 41, 2637-2643.	1.5	20
100	Characterization of distillability of entanglement in terms of positive maps. Physical Review A, 2005, 71, .	1.0	19
101	Remote sensing and in situ measurements of methane and ammonia emissions from a megacity dairy complex: Chino, CA. Environmental Pollution, 2017, 221, 37-51.	3.7	19
102	A sulfur dioxide Covariance-Based Retrieval Algorithm (COBRA): application to TROPOMI reveals new emission sources. Atmospheric Chemistry and Physics, 2021, 21, 16727-16744.	1.9	19
103	Acetone Atmospheric Distribution Retrieved From Space. Geophysical Research Letters, 2019, 46, 2884-2893.	1.5	18
104	Ten-Year Assessment of IASI Radiance and Temperature. Remote Sensing, 2020, 12, 2393.	1.8	18
105	On independent permutation separability criteria. Quantum Information and Computation, 2006, 6, 277-288.	0.1	18
106	Model simulations of the chemical and aerosol microphysical evolution of the Sarychev Peak 2009 eruption cloud compared to in situ and satellite observations. Atmospheric Chemistry and Physics, 2018, 18, 3223-3247.	1.9	17
107	Stratospheric aerosol radiative forcing simulated by the chemistry climate model EMAC using Aerosol CCI satellite data. Atmospheric Chemistry and Physics, 2018, 18, 12845-12857.	1.9	17
108	Complex refractive index of volcanic ash aerosol in the infrared, visible, and ultraviolet. Applied Optics, 2020, 59, 884.	0.9	17

#	Article	IF	CITATIONS
109	Temporal variations of flux and altitude of sulfur dioxide emissions during volcanic eruptions: implications for long-range dispersal of volcanic clouds. Atmospheric Chemistry and Physics, 2015, 15, 8381-8400.	1.9	16
110	Monthly Patterns of Ammonia Over the Contiguous United States at 2â€km Resolution. Geophysical Research Letters, 2021, 48, e2020GL090579.	1.5	16
111	Large-scale particulate air pollution and chemical fingerprint of volcanic sulfate aerosols from the 2014–2015 Holuhraun flood lava eruption of Bárðarbunga volcano (Iceland). Atmospheric Chemistry and Physics, 2019, 19, 14253-14287.	1.9	15
112	Constraints on eruption processes and event masses for the 2016–2017 eruption of Bogoslof volcano, Alaska, through evaluation of IASI satellite SO2 masses and complementary datasets. Bulletin of Volcanology, 2020, 82, 1.	1.1	15
113	Instantaneous longwave radiative impact of ozone: an application on IASI/MetOp observations. Atmospheric Chemistry and Physics, 2015, 15, 12971-12987.	1.9	14
114	Infrared Sounding of Volcanic Ash. , 2016, , 189-215.		14
115	Cross-validation of IASI/MetOp derived tropospheric Î'D with TES and ground-based FTIR observations. Atmospheric Measurement Techniques, 2015, 8, 1447-1466.	1.2	13
116	Validation of ash optical depth and layer height retrieved from passive satellite sensors using EARLINET and airborne lidar data: the case of the Eyjafjallajökull eruption. Atmospheric Chemistry and Physics, 2016, 16, 5705-5720.	1.9	13
117	Atmospheric Impacts of COVID-19 on NOx and VOC Levels over China Based on TROPOMI and IASI Satellite Data and Modeling. Atmosphere, 2021, 12, 946.	1.0	13
118	Present and future land surface and wet bulb temperatures in the Arabian Peninsula. Environmental Research Letters, 2022, 17, 044029.	2.2	13
119	Simulation of organics in the atmosphere: evaluation of EMACv2.54 with the Mainz Organic Mechanism (MOM) coupled to the ORACLE (v1.0) submodel. Geoscientific Model Development, 2022, 15, 2673-2710.	1.3	13
120	Distributions and seasonal variations of tropospheric ethene (C <sub>2</sub> H <sub>4</sub> ) from Atmospheric Chemistry Experiment (ACEâ€FTS) solar occultation spectra. Geophysical Research Letters, 2009, 36, .	1.5	12
121	Measurements of hydrogen cyanide (HCN) and acetylene (C <sub>2</sub> H <sub>2</sub> ) from the Infrared Atmospheric Sounding Interferometer (IASI). Atmospheric Measurement Techniques, 2013, 6, 917-925.	1.2	12
122	IASI-derived NH <sub>3</sub> enhancement ratios relative to CO for the tropical biomass burning regions. Atmospheric Chemistry and Physics, 2017, 17, 12239-12252.	1.9	12
123	Tropospheric Volcanic SO2 Mass and Flux Retrievals from Satellite. The Etna December 2018 Eruption. Remote Sensing, 2021, 13, 2225.	1.8	11
124	The Diel Cycle of NH <sub>3</sub> Observed From the FYâ€4A Geostationary Interferometric Infrared Sounder (GIIRS). Geophysical Research Letters, 2021, 48, e2021GL093010.	1.5	11
125	Do alternative inventories converge on the spatiotemporal representation of spring ammonia emissions in France?. Atmospheric Chemistry and Physics, 2020, 20, 13481-13495.	1.9	11
126	Current challenges in modelling far-range air pollution induced by the 2014–2015 Bárðarbunga fissure eruption (Iceland). Atmospheric Chemistry and Physics, 2016, 16, 10831-10845.	1.9	10

#	Article	IF	CITATIONS
127	Artificial Neural Networks to Retrieve Land and Sea Skin Temperature from IASI. Remote Sensing, 2020, 12, 2777.	1.8	10
128	Validation of mobile in situ measurements of dairy husbandry emissions by fusion of airborne/surface remote sensing with seasonalÂcontext from the Chino Dairy Complex. Environmental Pollution, 2018, 242, 2111-2134.	3.7	9
129	Identification of Short and Longâ€Lived Atmospheric Trace Gases From IASI Space Observations. Geophysical Research Letters, 2021, 48, e2020GL091742.	1.5	9
130	Analysis of atmospheric ammonia over South and East Asia based on the MOZART-4 model and its comparison with satellite and surface observations. Atmospheric Chemistry and Physics, 2021, 21, 6389-6409.	1.9	8
131	Convergent evidence for the pervasive but limited contribution of biomass burning to atmospheric ammonia in peninsular Southeast Asia. Atmospheric Chemistry and Physics, 2021, 21, 7187-7198.	1.9	8
132	The impact of organic pollutants from Indonesian peatland fires on the tropospheric and lower stratospheric composition. Atmospheric Chemistry and Physics, 2021, 21, 11257-11288.	1.9	8
133	Trends in spectrally resolved outgoing longwave radiation from 10 years of satellite measurements. Npj Climate and Atmospheric Science, 2021, 4, .	2.6	8
134	EUNADICS-AV early warning system dedicated to supporting aviation in the case of a crisis from natural airborne hazards and radionuclide clouds. Natural Hazards and Earth System Sciences, 2021, 21, 3367-3405.	1.5	8
135	On the Schmidt robustness of pure states. Journal of Physics A, 2006, 39, 4239-4249.	1.6	7
136	Acetylene (C <sub>2</sub> H <sub>2</sub> ) and hydrogen cyanide (HCN) from IASI satellite observations: global distributions, validation, and comparison with model. Atmospheric Chemistry and Physics, 2015, 15, 10509-10527.	1.9	7
137	First retrievals of peroxyacetyl nitrate (PAN) from ground-based FTIR solar spectra recorded at remote sites, comparison with model and satellite data. Elementa, 2021, 9, .	1.1	7
138	Multiscale observations of NH <sub>3</sub> around Toronto, Canada. Atmospheric Measurement Techniques, 2021, 14, 905-921.	1.2	7
139	Spectrally Resolved Fluxes from IASI Data: Retrieval Algorithm for Clear-Sky Measurements. Journal of Climate, 2020, 33, 6971-6988.	1.2	7
140	Ground-based measurements of atmospheric NH3 by Fourier transform infrared spectrometry at Hefei and comparisons with IASI data. Atmospheric Environment, 2022, 287, 119256.	1.9	6
141	The disentangling power of unitaries. Physics Letters, Section A: General, Atomic and Solid State Physics, 2007, 365, 400-402.	0.9	5
142	Using satelliteâ€based measurements to explore spatiotemporal scales and variability of drivers of new particle formation. Journal of Geophysical Research D: Atmospheres, 2016, 121, 12217-12235.	1.2	5
143	Ammonia Emissions from Mudflats of River, Lake, and Sea. ACS Earth and Space Chemistry, 2020, 4, 614-619.	1.2	5
144	Continental and Ecoregion‧pecific Drivers of Atmospheric NO <sub>2</sub> and NH <sub>3</sub> Seasonality Over Africa Revealed by Satellite Observations. Global Biogeochemical Cycles, 2021, 35, e2020GB006916.	1.9	5

#	Article	IF	CITATIONS
145	A multi-sensor satellite-based archive of the largest SO <sub>2</sub> volcanic eruptions since 2006. Earth System Science Data, 2020, 12, 3139-3159.	3.7	5
146	Volcanic SO <sub>2</sub> layer height by TROPOMI/S5P: evaluation against IASI/MetOp and CALIOP/CALIPSO observations. Atmospheric Chemistry and Physics, 2022, 22, 5665-5683.	1.9	5
147	Estimating exposure to hydrogen sulfide from animal husbandry operations using satellite ammonia as a proxy: Methodology demonstration. Science of the Total Environment, 2020, 709, 134508.	3.9	4
148	Investigating the Large-Scale Transport of a Volcanic Plume and the Impact on a Secondary Site. Atmosphere, 2020, 11, 548.	1.0	4
149	IASIâ€Derived Sea Surface Temperature Data Set for Climate Studies. Earth and Space Science, 2021, 8, e2020EA001427.	1.1	4
150	Operational Integration of Spaceborne Measurements of Lava Discharge Rates and Sulfur Dioxide Concentrations for Global Volcano Monitoring. Advanced Technologies in Earth Sciences, 2014, , 307-331.	0.9	4
151	Changes in biomass burning, wetland extent, or agriculture drive atmospheric NH <sub>3</sub> trends in select African regions. Atmospheric Chemistry and Physics, 2021, 21, 16277-16291.	1.9	3
152	A space view of agricultural and industrial changes during the Syrian civil war. Elementa, 2021, 9, .	1.1	3
153	Variability of the Aerosol Content in the Tropical Lower Stratosphere from 2013 to 2019: Evidence of Volcanic Eruption Impacts. Atmosphere, 2022, 13, 250.	1.0	3
154	Time evolution of temperature profiles retrieved from 13 years of infrared atmospheric sounding interferometer (IASI) data using an artificial neural network. Atmospheric Measurement Techniques, 2022, 15, 1779-1793.	1.2	3
155	Observation of Air Pollution over China Using the IASI Thermal Infrared Space Sensor. , 2017, , 309-322.		2
156	The 2015 Calbuco Volcanic Cloud Detection Using GNSS Radio Occultation and Satellite Lidar. , 2020, , .		2
157	Understanding the Simulated Ammonia Increasing Trend from 2008 to 2015 over Europe with CHIMERE and Comparison with IASI Observations. Atmosphere, 2022, 13, 1101.	1.0	2
158	Atmospheric Composition Applications with IASI and next-generation hyperspectral infrared sounders (IASI-NG and IRS). , 2021, , .		1
159	IASI/MetOp sounder contribution for atmospheric composition monitoring: 4-year study of radiance data. , 2013, , .		Ο
160	Validation of ASH Optical Depth and Layer Height from IASI using Earlinet Lidar Data. EPJ Web of Conferences, 2016, 119, 07006.	0.1	0
161	Prototyping of a Multi-Hazard Early Warning System for Aviation and Development of NRT Alert Products within the EUNADICS-AV and OPAS Projects. , 2020, , .		Ο